Article

Integrated Transcriptome and Metabolome Analysis Reveals an Essential Role for Auxin in Hypocotyl Elongation during End-of-Day Far-Red Treatment of *Cucurbita moschata* (Duch. Ex Lam.)

Qi Liu [1,2], Hanqing Zhang [3], Yanhao Mei [1,2], Qi Li [1,2], Yahui Bai [1,2], Huibin Yu [1,2], Xiaodong Xu [1,2], Jianxiang Ma [1], Yongjun Wu [3,*] and Zhenchao Yang [1,2,*]

1   College of Horticulture, Northwest A & F University, Yangling 712100, China; lq821798304@163.com (Q.L.); meiyanhao2318@163.com (Y.M.); lq13289386001@163.com (Q.L.); byh31886@163.com (Y.B.); 18879325352@163.com (H.Y.); 15076029709@163.com (X.X.); majianxiang@126.com (J.M.)
2   Key Laboratory of Protected Horticultural Engineering in Northwestern China, Ministry of Agriculture and Rural Affairs, Northwest A & F University, Yangling 712100, China
3   College of Life Sciences, Northwest A & F University, Yangling 712100, China; z1872821428@163.com
*   Correspondence: wuyongjun@nwafu.edu.cn (Y.W.); yangzhenchao@126.com (Z.Y.)

Abstract: Long, robust hypocotyls are important for facilitating greenhouse transplant production. The use of far-red light at the end of the day (end-of-day far-red, EOD-FR) is known to prompt hypocotyl elongation, but the mechanism of EOD-FR-mediated hypocotyl elongation in pumpkin remains unclear. Here, we found that hypocotyl length, parenchymal cell size in hypocotyls, and plant IAA levels were significantly greater in pumpkin after EOD-FR treatment. This effect was counteracted by the application of the polar auxin transport inhibitor 1-N-naphthylphthalamic acid. Integrated transcriptomic and metabolomic analysis of pumpkin hypocotyls revealed that the expression of auxin-related genes changed significantly after EOD-FR treatment, and the contents of the auxin biosynthetic precursors tryptophan and indole were also significantly higher. Our results show that auxin plays an essential role in EOD-FR-mediated hypocotyl elongation, shed light on the mechanisms of EOD-FR mediated hypocotyl elongation, and provide a theoretical basis for the use of EOD-FR in facility cultivation.

Keywords: *Cucurbita moschata* (Duch. ex Lam.); far-red light; auxin; transcriptome; metabolomics

1. Introduction

Light is essential for plant growth and development, serving as an energy source for photosynthesis and as an environmental cue for photomorphogenesis [1]. In recent years, artificial light sources have become a new type of 'intelligent' equipment in agricultural production facilities, particularly for vegetable production [2]. In the external light environment, different wavelengths of light have specific effects on plant growth and development, and studies have shown that the ratio of red to far red light (R:FR) has a particularly important effect on plant morphology [3,4]. Many researchers have found that the use of far-red light at the end of the day (EOD-FR) significantly promotes hypocotyl elongation in *Arabidopsis*, pumpkin, tomato, watermelon and other plants [1,5–9].

In vegetable grafting propagation, the use of rootstocks with long hypocotyls and uniform growth can improve grafting speed and prevent vulnerable scions from coming into contact with the soil during and after transplant [10]. Pumpkin, a vegetable crop in the *Cucurbitaceae*, has a strong root system and good disease and stress resistance; it is therefore widely used as a rootstock for the grafting of melons [11]. Previous studies have shown that EOD-FR mediates the hypocotyl elongation of pumpkin without affecting plant dry weight, stem diameter, or seedling index. There is some flexibility in the selection

of FR light intensity and duration to provide a sufficient FR light dose (light intensity $\times$ duration) [6].

These results indicate that EOD-FR has potential value for the facility cultivation of vegetable rootstocks. However, the mechanism of EOD-FR mediated hypocotyl elongation in pumpkin has not been reported. In *Arabidopsis*, hypocotyl elongation mediated by low R:FR is inhibited in mutants with low auxin levels or disrupted auxin transport [12,13]. This indicates that auxin is an important factor mediating the morphological changes in *Arabidopsis* in a low R:FR environment, but it remains unclear whether auxin plays a similar role in EOD-FR-mediated elongation of pumpkin hypocotyls. With the rapid evolution of next-generation sequencing strategies and decreases in sequencing costs, transcriptome sequencing has become an effective way to explore the molecular mechanisms that underlie biological phenomena [14,15]. However, the complexities of auxin response involve the modulation of both transcriptional and metabolic networks, and the use of RNA-seq alone may be insufficient to identify the central metabolic pathways and pivotal reactions that underlie this phenomenon [16].

In recent years, the use of metabolomics techniques for the quantitative analysis of small molecular weight plant metabolites has become increasingly widespread. These techniques enable researchers to explore the relationships between metabolite levels and phenotypic changes, providing new insights into multiple phenomena [17].

In this study, we performed EOD-FR treatment on pumpkin seedlings with and without 1-N-naphthylpthalamic acid (NPA) and measured their hypocotyl lengths and IAA levels. We combined RNA-seq and metabolite profiling of pumpkin hypocotyls to measure changes in auxin-related genes and metabolites, and we verified the expression of selected genes by qRT–PCR. Our study shows that auxin plays an important role in EOD-FR-mediated hypocotyl elongation of pumpkin.

2. Methods

2.1. Plant Materials and Sample Collection

The *Cucurbita moschata* (Duch. ex Lam.) variety 'Yong an 4' was provided by the Shaanxi Academy of Agricultural Sciences (Certification number 2010001, Shaanxi Vegetable Registration) for use in the following experiments. Seeds were sown into a 50-hole seedling plate and grown in seedling substrate (Lvyuan seedling substrate, Yufeng Co., Ltd., Yangling, China) under artificial light (14 h light at 28 °C, 10 h dark at 18 °C). After 3 days, when their hypocotyl hooks had emerged and straightened and their cotyledons were fully unfolded, seedlings of uniform size were selected for use in the experiment. Four different treatments were applied: far-red light (treatment, T), far-red light plus the auxin polar transport inhibitor NPA (NPA-T), no far-red light or NPA (Control, CK), and NPA only (NPA-CK). CK and NPA-CK did not receive far-red treatment and were placed in the dark. Twenty seedlings were used for each treatment, and the treatment durations and intensities are shown in Table 1.

Table 1. Far-red light intensity (photon flux), duration, and applied far-red dose of the end-of-day far-red (EOD-FR) light.

Treatment	Duration(s)	FR Photo Flux (μmmol·m^{-2}·s^{-1})	FR Dose (mmol·m^{-2}·d^{-1})
CK	0	0	0
T	120	34	4.08
NPA-T	120	34	4.08
NPA-CK	0	0	0

We prepared a paste of NPA in lanolin (50 μmol NPA/g) according to the method of Jouve [18]. NPA powder and a small amount of dimethyl sulfoxide were added to lanolin, which was then melted by placing its glass container in water for about a minute and stirring with a glass rod. The NPA paste was applied to the hypocotyl 30 min before EOD-FR treatment. Hypocotyl lengths of all plants were measured daily with a steel ruler. After 6 days of treatment, plants were randomly selected for measurement of plant height, stem diameter, and dry and fresh weights of above- and belowground parts and for the preparation of hypocotyl paraffin sections. Plant dry weights were determined after drying completely at 55 °C for 72 h in a drying oven (DHG-140L, Youke Instrument Equipment Co., Ltd., Hefei, China). The leaves and hypocotyls of eight plants were rapidly cut and frozen in liquid nitrogen for subsequent RNA sequencing and metabolite detection.

2.2. Auxin Quantification

Auxin quantification was performed as described by Du et al. [19] with minor modifications. Plant tissues were frozen in liquid nitrogen and crushed into a powder, then extracted with 1 mL methanol/water/formic acid (15:4:1, v/v/v). The combined extracts were evaporated to dryness under a nitrogen gas stream, reconstituted in 100 μL 80% methanol (v/v), and filtered through a nylon syringe filter (ANPLE, 13 mm $\times$ 0.22 μm) for use in LC-MS/MS analysis. The sample extracts were analyzed using an LC-ESI-MS/MS system. In brief, the mobile phase consisted of acetonitrile (solvent A) and 0.02% (v/v) glacial acetic acid in water (solvent B). The samples were purified using a C-18 column and an ACQUITY I-CLASS liquid chromatography system (Waters) and finally measured by mass spectrometry (AB SCIEX Analyst, QTRAP 5500). IAA standards (CAS 87-51-4, Sigma, St. Louis, MO, USA) were used to optimize the mass spectrometry parameters and fragment spectra. A standard curve with a regression coefficient > 0.99 was used to calculate IAA and Me-IAA levels (Figure S1).

2.3. Metabolomic Profiling

Freeze-dried powdered samples (0.1 g) were extracted with 50% methanol, then centrifuged at $4000\times$ *g* and 4 °C before filtering. All chromatographic separations were performed using an ultra-performance liquid chromatography (UPLC) system (SCIEX, UK). An ACQUITY UPLC T3 column (100 $\times$ 2.1 mm, 1.8 μm, Waters, UK) was used for the reversed phase separation. A high-resolution tandem mass spectrometer (TripleTOF 5600+, SCIEX, UK) was used to detect metabolites eluted from the column. The acquired MS data were pre-processed with XCMS software. LC-MS raw data files were converted into mzXML format and then processed using XCMS, CAMERA, and metaX toolbox implemented in R software. Each ion was identified based on retention time (RT) and m/z. The MS fragment data from the mass spectrometer were matched with a secondary library of in-house metabolite standards, and metabolites with similarity >80% were extracted. An online database was used to annotate the metabolites by matching the exact molecular mass data (m/z) of the samples with those from the database. Statistical analysis was performed using Student's t-test with a multiple testing correction to obtain Q-values for individual metabolites, and VIP values were obtained using partial least squares discriminant analysis. Significantly different metabolites were identified using thresholds of > 2-fold difference, Q < 0.05, and variable importance projection (VIP) > 1.

2.4. Transcriptome Sequencing and Identification of DEGs

CK and T were selected for RNA-seq analysis. Total RNA was extracted using the TRIzol reagent (Invitrogen, Carlsbad, CA, USA) and reverse-transcribed to create six cDNA libraries using the protocol for the TruSeq Stranded mRNA Library Prep Kit (Illumina, San Diego, CA, USA). Paired-end sequencing was performed on an Illumina HiSeq 4000 instrument (LC-Bio Technology CO., Ltd., Hangzhou, China). Gene expression levels were calculated as fragments per kilobase per million reads [20]. Differentially expressed genes were identified based on thresholds of log2 (fold change) >1 or <−1 and *p* < 0.05.

We annotated the DEGs by performing BLAST searches against three public databases: NR, Non-Redundant Protein Sequence Database; GO, Gene Ontology; and KEGG, Kyoto Encyclopedia of Genes and Genomes. GO terms or KEGG pathways with a Bonferroni-corrected *p*-value < 0.05 were considered to be significantly enriched in the differentially expressed gene set.

2.5. Quantitative Real-Time PCR (qRT–PCR)

Gene-specific primers were designed based on the sequences obtained from RNA-seq data (Table S1). PCR reactions were carried out in 96-well plates (20 μL per well) in a reaction buffer that contained 10 μL SuperReal PreMix Plus (SYBR Green) (Monad), 0.5 μL of each forward and reverse primer, 2 μL cDNA template, and 7 μL RNase-Free ddH2O. PCR was performed using the ABI QuantStudio 6 Flex (Applied Biosystems, Carlsbad, CA, USA) with 39 cycles of 95 °C for 30 s, 60 °C for 5 s, and 95 °C for 30 s. At the end of the reaction, the dissociation curve was analyzed, and the specificity of the primers was evaluated. Relative gene expression levels were calculated using the $2^{-\Delta\Delta Ct}$ method [21]. All reactions in all experiments were repeated three times.

2.6. Preparation and Observation of Hypocotyl Paraffin Sections

Hypocotyls were fixed in FAA (3.7% formaldehyde, 5% acetic acid, and 50% ethanol by volume) for 24 h under vacuum, then dehydrated in an ethanol series (70, 80, and 90%) and processed as described previously [22]. Wax blocks were sectioned at 10 μm. Safranin-O/fast-green staining was performed using a kit following the manufacturer's instructions (Wuhan Google Bio-Technology Co., Wuhan, China). A research-grade upright fluorescence microscope (BX51, Olympus Corporation, Tokyo, Japan) was used to observe and photograph the cells at 20× magnification with CellSens Standard software.

2.7. Statistical Analysis

All data were analyzed using GraphPad Prism 8, Microsoft Excel 2013, and SPSS 19.0; they are expressed as mean ± SD. Treatments were compared using Student's t-test, and *p*-values < 0.05 were considered statistically significant.

3. Results

3.1. Effects of EOD-FR on Growth, Hypocotyl Cell Morphology, and Auxin Levels of Pumpkin Seedlings

Hypocotyls were significantly longer in EOD-FR-treated plants than in control plants (Figure 1A). However, there were no significant differences in stem diameter or above- and belowground fresh and dry weights between the controls (CK) and the seedlings treated with far-red light (T). Observation of axial sections of hypocotyl cells (Figure 1J–K) revealed that the parenchyma cells had expanded significantly after EOD-FR treatment (Figure 1H–J). Hypocotyl elongation, stem diameter, dry and fresh weights, and cell expansion decreased significantly after treatment with the polar auxin transport inhibitor NPA (Figure 1H–J).

(**A**)
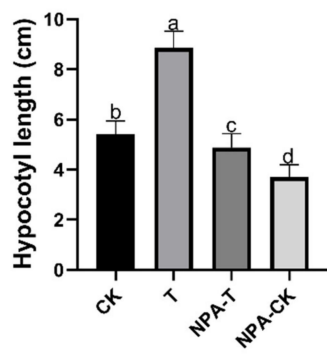
(**B**)
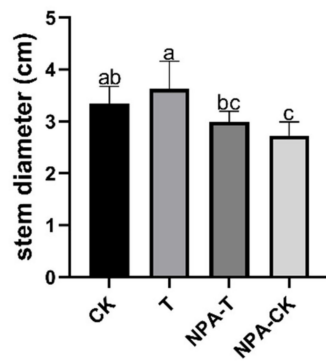
(**C**)

(**D**)

(**E**)

(**F**)

(**G**)

Figure 1. *Cont.*

(**H**)

(**I**)

(**J**)

(**K**)

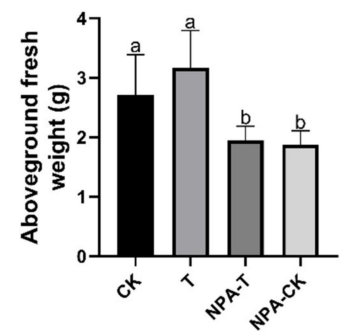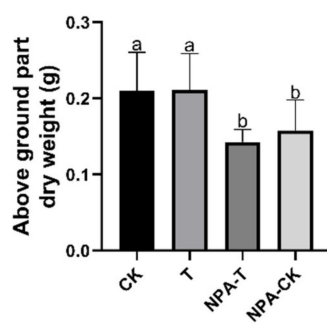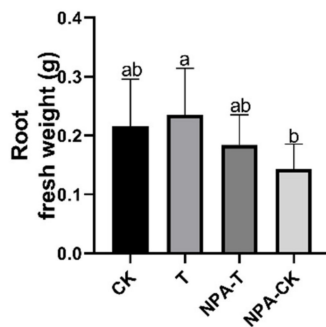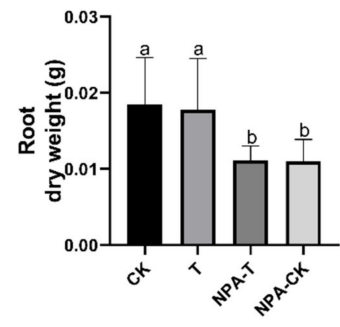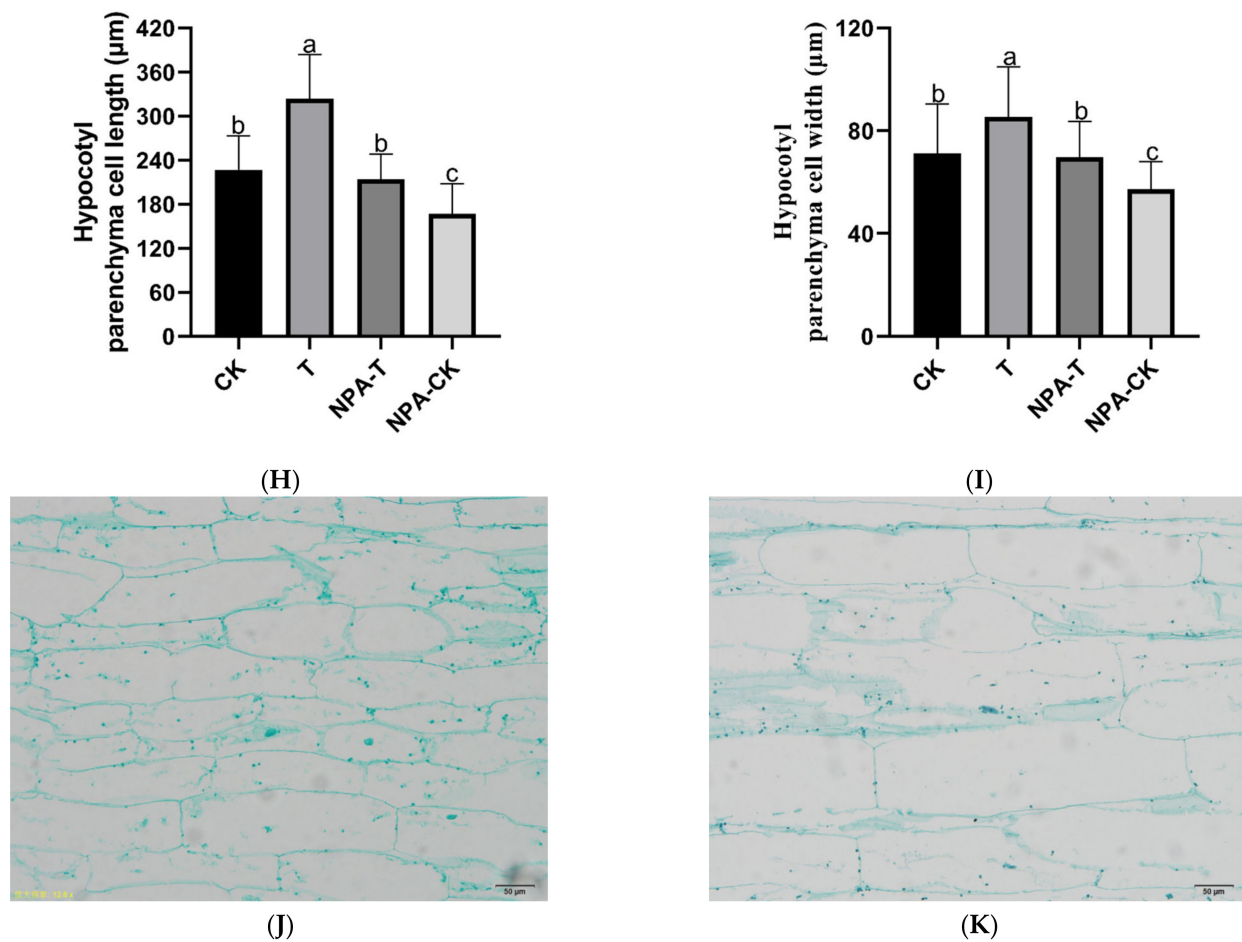**Figure 1.** Phenotypic changes in pumpkin seedlings in response to EOD-FR treatment. CK, Control; T, EOD-FR treatment; NPA-T, EOD-FR treatment plus the auxin transport inhibitor NPA; NPA-CK, NPA alone. (**A**) Pumpkin seedlings from different treatments. Hypocotyl length (**B**), stem diameter (**C**), shoot system fresh weight (**D**), root fresh weight (**E**), shoot system dry weight (**F**), and root dry weight (**G**) of pumpkin seedlings from different treatments. Observations of hypocotyl cells in pumpkin seedlings during EOD-FR treatment. Changes in length (**H**) and width (**I**) of parenchyma cells in different treatments. Morphological changes in hypocotyl cells of different treatments (**J,K**). Different lowercase letters denote significant differences ($p < 0.05$), and error bars indicate SD values.

3.2. Changes in Auxin Level after EOD-FR Treatment

Using LC-MS, we found that IAA levels in hypocotyls of the T seedlings were significantly higher than those of other treatments (Figure 2), suggesting that IAA was involved in cell elongation and cell wall remodeling in the hypocotyl of pumpkin. The level of IAA decreased after NPA was applied. The IAA content in leaves increased significantly after EOD-FR treatment, and the IAA content in leaves of the NPA-T group was the highest. When NPA was applied alone, the IAA content of leaves and hypocotyls decreased significantly.

Furthermore, we found that the hypocotyl of pumpkin accumulated more methylindole-3-acetic acid (Me-IAA) after EOD-FR treatment (Figure S2). However, there was no significant difference in Me-IAA content between CK and T leaves. The content of Me-IAA in leaves and hypocotyls of NPA-CK was significantly lower than that of other treatments (Figure S2).
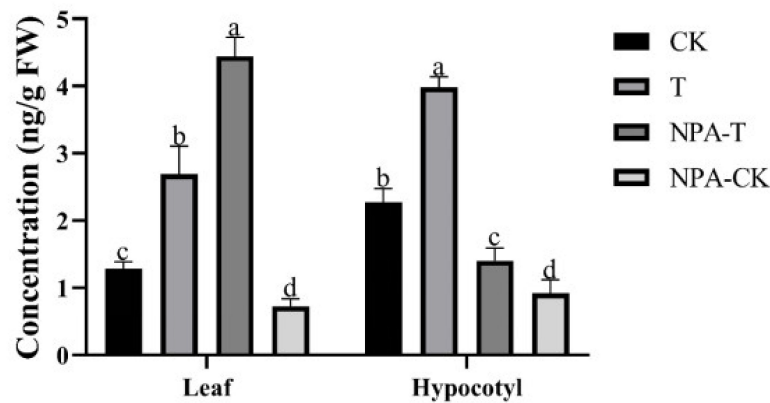
Figure 2. IAA levels in different treatments. Error bars represent $\pm$ SD. Different letters denote significant differences ($p < 0.05$).

3.3. Metabolomics Analyses and Identification of Differentially Abundant Metabolites

To investigate the metabolites related to IAA synthesis in hypocotyls under EOD-FR, we analyzed their metabolic profiles using LC-MS. A principal component analysis (PCA) model was used (Figure S3) to study the relationships between metabolite levels and EOD-FR. Based on PCA analysis of metabolites identified in the positive and negative ion modes, we found that metabolite accumulation in hypocotyls differed markedly between CK and T.

Compared with CK, T accumulated more L-tryptophan (C00078), tryptophan (C00806), and indole (C00463). In particular, the content of L-tryptophan increased 2.14-fold, and that of tryptophan increased 2.06-fold. The content of 3-indole acrylic acid (IAcrA) [23], 3-methylindole (C08313), and indole-3-carboxaldehyde (C08493), other products of the tryptophan metabolic pathway, also increased significantly after EOD-FR treatment (Table S2).

3.4. RNA-Seq Analysis

The sizes of the sequenced RNA-seq libraries ranged from 40, 704, 360 bp to 54, 037, 758 bp (Table S3), and the Q30 percentage (percentage of sequences with an error rate <0.1%) was greater than 93% for each library. Overall, the RNA-seq data were of high quality and could be used for further analysis.

3.5. GO and KEGG Enrichment Analysis of Differentially Expressed Genes

Analysis of differentially expressed genes (DEGs) revealed that 1968 genes were upregulated, and 833 genes were downregulated in hypocotyls after EOD-FR treatment (Table S4, Figures S4 and S5). GO enrichment analysis of upregulated genes (Table S5 and Figure S6) indicated that GO terms related to cell division and cell wall metabolism were significantly enriched; cell wall biogenesis, plant-type cell wall, and cell wall were among the top 20 enriched GO terms.

The metabolic pathways associated with the DEGs were explored further by KEGG enrichment analysis. The KEGG enrichment scatterplot showed that starch and sucrose metabolism (K00500) and amino sugar and nucleotide sugar metabolism (K00520) were the two pathways with the highest degree of enrichment. Sixty-four and 44 genes were involved in these two pathways, respectively (Table S6 and Figure S7).

3.6. Identification of Auxin-Related DEGs

We identified 19 auxin-related DEGs in the RNA-seq data, and their expression levels are presented in the form of a heatmap (Figure 3A). These genes were involved in the metabolism and transport of auxin in pumpkin hypocotyls. Tryptophan aminotransferase-related protein 2 (TAR2) and two flavin-containing monooxygenases (YUCCA8 and FMO GS-OX-like 9) associated with auxin synthesis were upregulated after EOD-FR treatment.

An N-(5-phosphate ribose) o-aminobenzoate isomerase 1 gene, which encodes a key enzyme in tryptophan biosynthesis, was also significantly upregulated after EOD-FR treatment. Two additional genes involved in auxin homeostasis, indole-3-acetic acid-amido synthetase GH3.6 and IAA-amino acid hydrolase ILR1-like 3, were downregulated 9.35-fold and upregulated 2.02-fold, respectively. Eleven of the DEGs participated in auxin transport, including six influx carriers (two AUX-LIKE 1, one AUX-LIKE 2, two AUX-LIKE 3, and one AUX-LIKE 5), two efflux carriers (PIN 4 and PIN-LIKE 5), two homologs of ABC transporter B family member 19, one WALLS ARE THIN 1 (WAT1) transporter, and two CBL-interacting serine/threonine protein kinase 6 related (CIPK 6) genes.
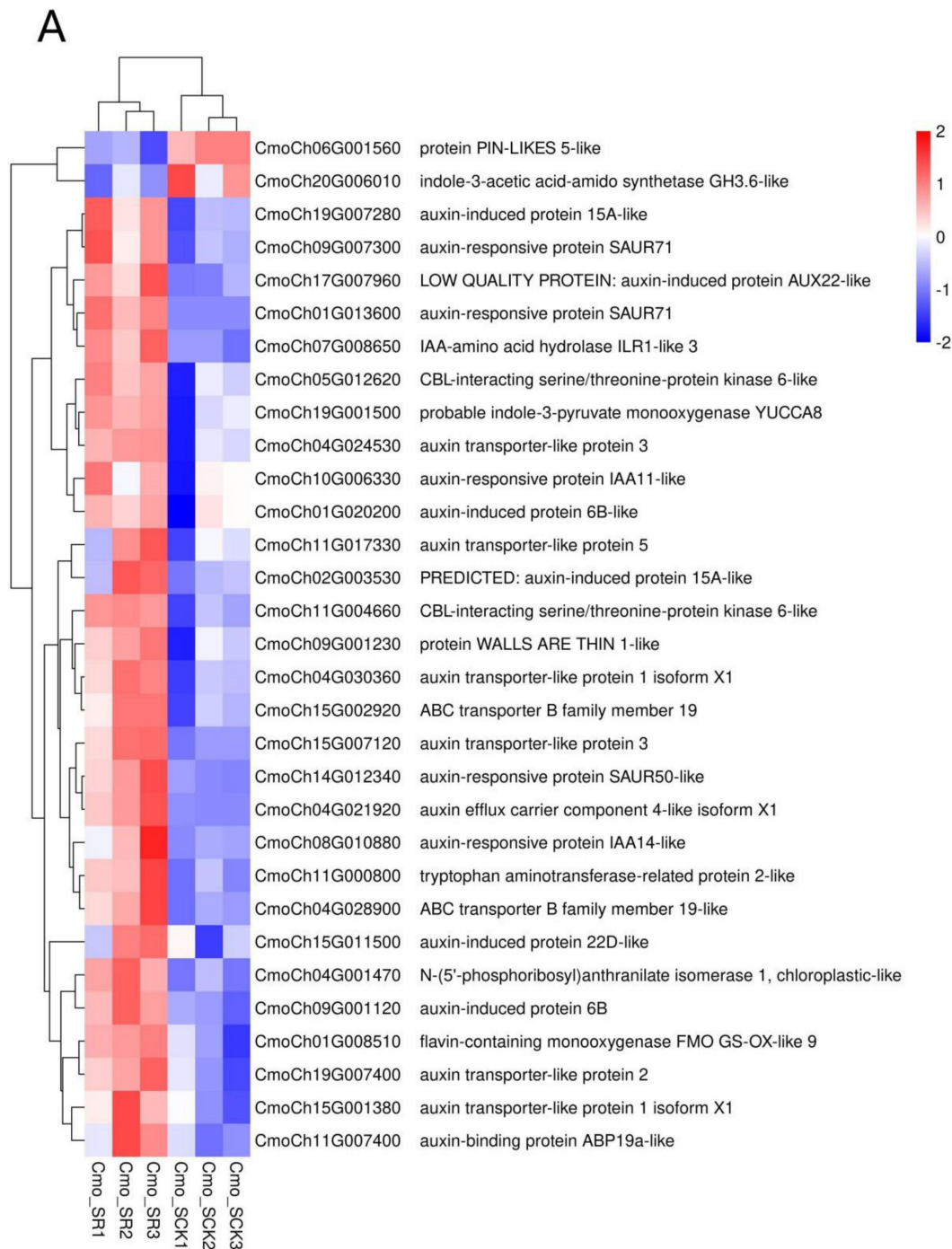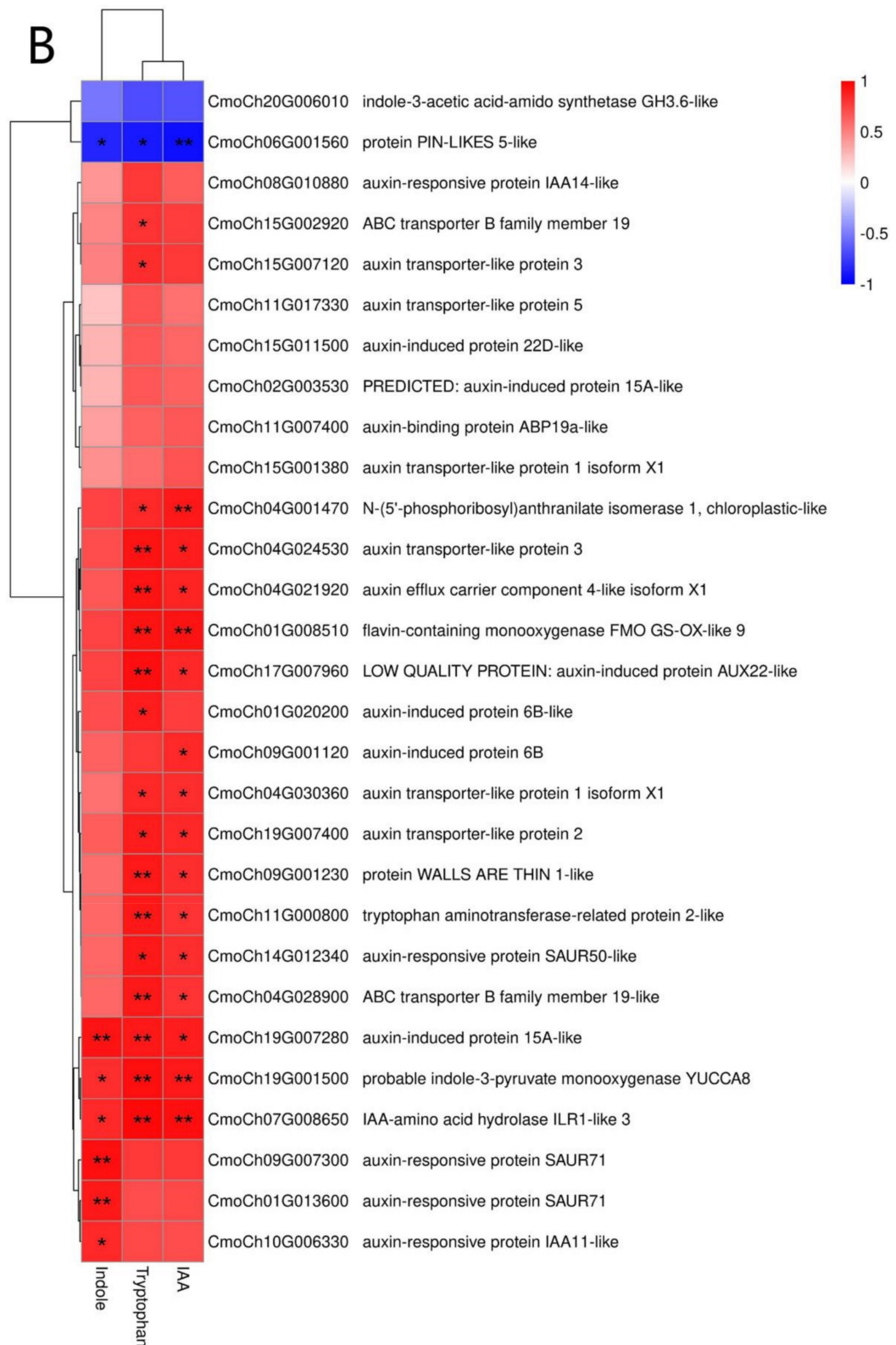

Figure 3. *Cont.*

B

Gene ID	Description	Indole	Tryptophan	IAA
CmoCh20G006010	indole-3-acetic acid-amido synthetase GH3.6-like			
CmoCh06G001560	protein PIN-LIKES 5-like	*	*	**
CmoCh08G010880	auxin-responsive protein IAA14-like			
CmoCh15G002920	ABC transporter B family member 19		*	
CmoCh15G007120	auxin transporter-like protein 3		*	
CmoCh11G017330	auxin transporter-like protein 5			
CmoCh15G011500	auxin-induced protein 22D-like			
CmoCh02G003530	PREDICTED: auxin-induced protein 15A-like			
CmoCh11G007400	auxin-binding protein ABP19a-like			
CmoCh15G001380	auxin transporter-like protein 1 isoform X1			
CmoCh04G001470	N-(5'-phosphoribosyl)anthranilate isomerase 1, chloroplastic-like		*	**
CmoCh04G024530	auxin transporter-like protein 3		**	*
CmoCh04G021920	auxin efflux carrier component 4-like isoform X1		**	*
CmoCh01G008510	flavin-containing monooxygenase FMO GS-OX-like 9		**	**
CmoCh17G007960	LOW QUALITY PROTEIN: auxin-induced protein AUX22-like		**	*
CmoCh01G020200	auxin-induced protein 6B-like		*	
CmoCh09G001120	auxin-induced protein 6B			*
CmoCh04G030360	auxin transporter-like protein 1 isoform X1		*	*
CmoCh19G007400	auxin transporter-like protein 2		*	*
CmoCh09G001230	protein WALLS ARE THIN 1-like		**	*
CmoCh11G000800	tryptophan aminotransferase-related protein 2-like		**	*
CmoCh14G012340	auxin-responsive protein SAUR50-like		*	*
CmoCh04G028900	ABC transporter B family member 19-like		**	*
CmoCh19G007280	auxin-induced protein 15A-like	**	**	*
CmoCh19G001500	probable indole-3-pyruvate monooxygenase YUCCA8	*	**	**
CmoCh07G008650	IAA-amino acid hydrolase ILR1-like 3	*	**	**
CmoCh09G007300	auxin-responsive protein SAUR71	**		
CmoCh01G013600	auxin-responsive protein SAUR71	**		
CmoCh10G006330	auxin-responsive protein IAA11-like	*		

Figure 3. (**A**) Expression heatmap of DEGs related to auxin response in pumpkin during EOD-FR treatment. (**B**) Heatmap of correlations between auxin-related DEGs and differentially accumulated auxin metabolites. * Correlation ≥ 0.8. ** Correlation ≥ 0.9.

### 3.7. Integrated Analysis of the Transcriptome and Metabolome

We calculated the Pearson correlation coefficients between the levels of indole, tryptophan, and IAA and the expression of auxin-related genes, and the results are presented as a heatmap in Figure 3B. The correlation coefficients between tryptophan and the expression of 16 genes were greater than 0.8, and ten of these genes had correlation coefficients greater than 0.9. Five genes had correlation coefficients greater than 0.8 with indole. Fourteen genes had correlation coefficients greater than 0.8 with IAA, and seven had correlation coefficients greater than 0.9. Based on these results and the reported auxin regulatory network from previous studies, we proposed the hypothetical EOD-FR response mechanism presented in Figure 4.
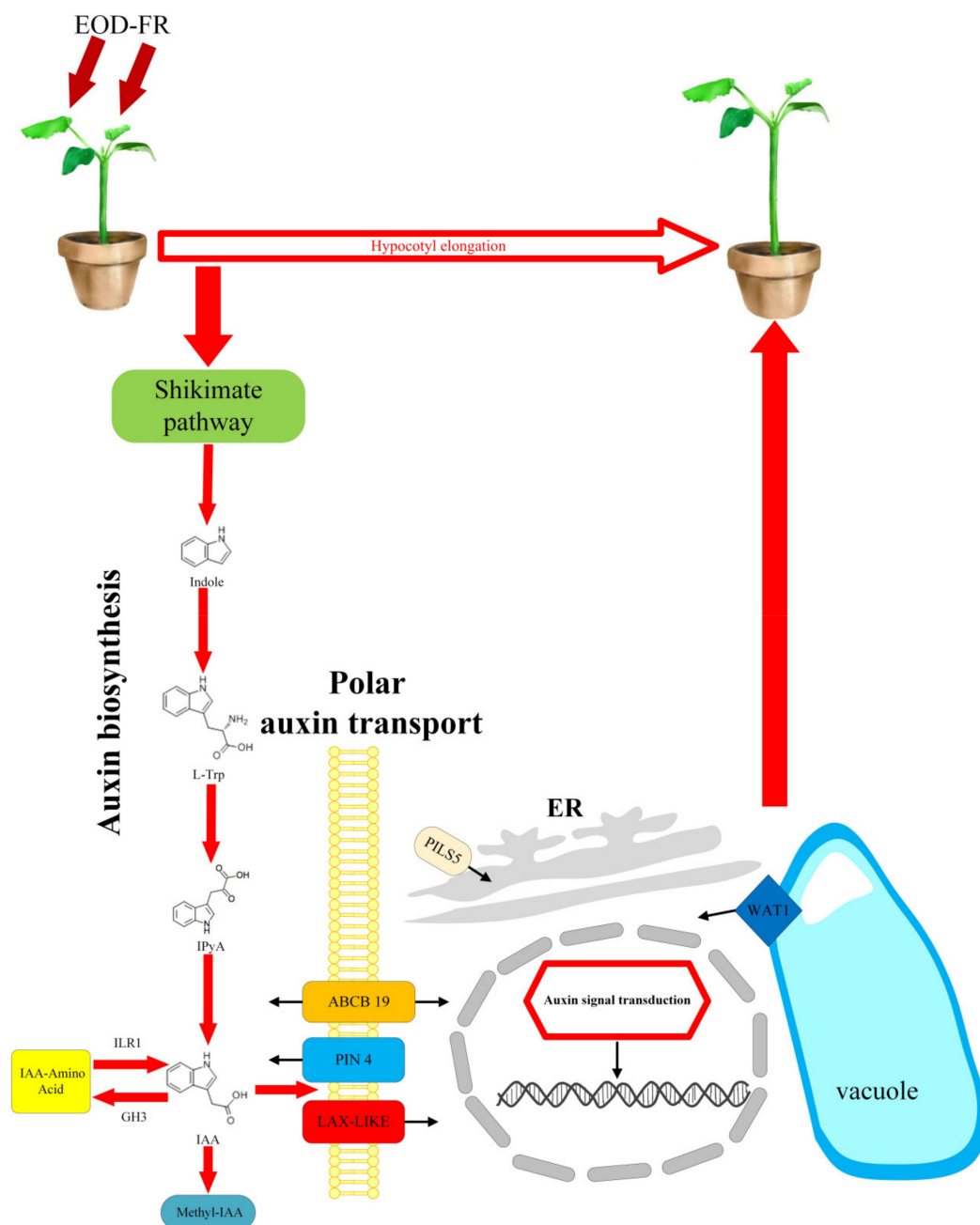
Figure 4. Hypothetical model of auxin-induced hypocotyl elongation in pumpkin under EOD-FR treatment. The figure depicts several auxin-related biological processes and reactions. Arrows indicate the directions of catalytic reactions or transport.

3.8. qRT–PCR

We selected six DEGs for qRT–PCR verification (Figure S8), and their relative expression levels measured with qRT–PCR were consistent with their FPKM values in the RNA-seq dataset ($R^2 = 0.8607$, $p < 0.01$) (Figure S9), indicating that the RNA-seq data were accurate. To verify the effect of auxin on gene expression, we selected eight auxin-related genes and measured their expression in the CK, T, NPA-T, and NPA-CK 4 treatments (Figure 5), the expression of these eight genes was clearly downregulated in response to the auxin transport inhibitor NPA.
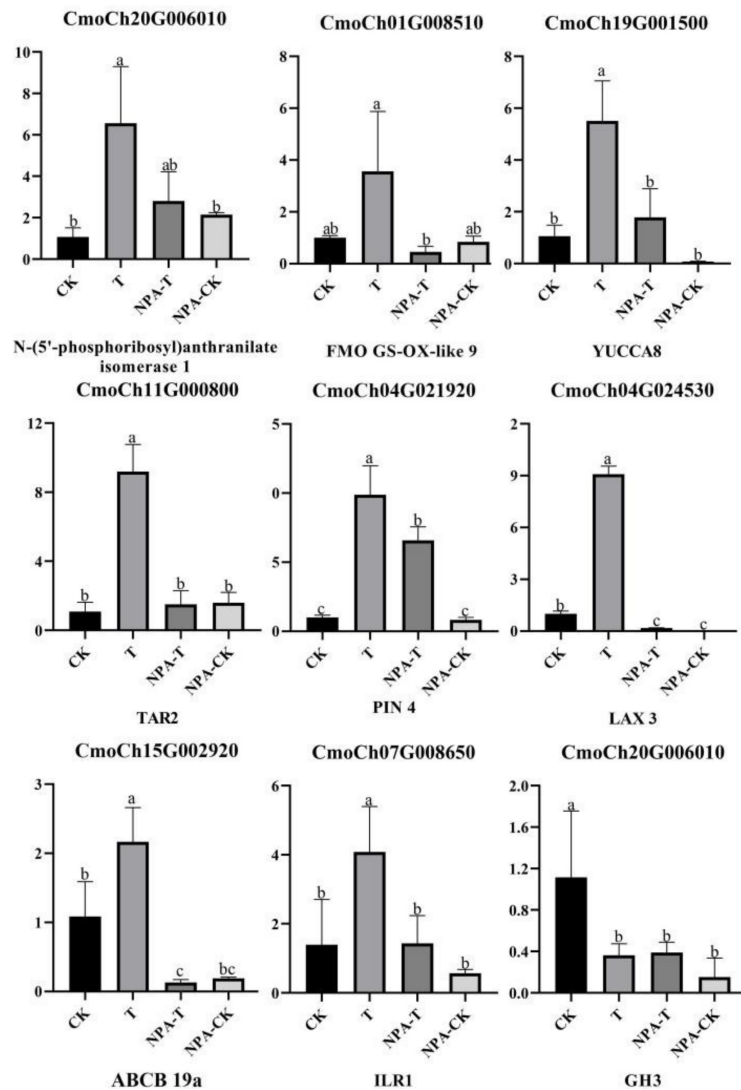
Figure 5. Expression of eight genes associated with hypocotyl elongation during EOD-FR treatment. Different lowercase letters indicate a significant difference at the 5% level between treatments.

4. Discussion

Emerging evidence indicates that auxin plays an important role in the regulation of plant elongation in a low R:FR environment [12,13]. Pumpkin is an important cash crop, but the specific mechanisms by which auxin mediates hypocotyl elongation in pumpkin in response to EOD-FR have not been characterized. In this study, application of the auxin polar transport inhibitor NPA counteracted EOD-FR-induced hypocotyl elongation (Figure 1A,B) and reduced IAA levels in the hypocotyls (Figure 2). Through transcriptome and metabolome analysis, we identified a number of auxin-related genes and metabolites whose levels changed in response to EOD-FR. This result suggested that the increased

auxin content of hypocotyls after EOD-FR treatment was an essential factor mediating their elongation. We integrated the transcriptome and metabolome data, and these results suggested that the increase in IAA was due to enhanced auxin synthesis, homeostasis, and transport to the hypocotyl.

Previous studies have found that the TAA-YUC pathway is the main pathway of auxin synthesis in *Arabidopsis* in response to low R:FR [12]. In this pathway, tryptophan aminotransferase of *Arabidopsis1* (TAA1) and TAA1-RELATED proteins (TARs) convert L-tryptophan to IPyA [24], and members of the flavin-containing monooxygenase (YUCCA) family then convert IPyA to IAA [25]. Research has shown that the IAA content of the *Arabidopsis* tar2-1 mutant is decreased [26] and that the yuc2yuc5yuc8yuc9 quadruple mutant is completely unable to respond to low R:FR [27]. YUCCA8 is thought to be the key auxin synthesis gene induced by low R:FR in *Arabidopsis* [28].

Using RNA-seq and qRT–PCR, we demonstrated that one TAR2 and two YUCCA (YUCCA8 and FMO GS-OX-like 9) genes were upregulated in pumpkin hypocotyls after EOD-FR treatment. At the same time, the content of L-tryptophan also increased after EOD-FR treatment. Previous studies have found that L-tryptophan is involved in many plant auxin biosynthetic pathways [29] and is an important precursor for auxin synthesis [30]. For example, IAA levels increased 57-fold in rice that exhibited excessive tryptophan synthesis [31,32]. Therefore, the three genes mentioned above participate in tryptophan-dependent IAA biosynthesis, and their upregulation may be an important reason for the increased IAA levels in pumpkin hypocotyls after EOD-FR treatment.

EOD-FR treatment also significantly increased indole content and the expression of a gene encoding N-(5′-phosphoribosyl) anthranilate isomerase 1, which catalyzes the third step in tryptophan biosynthesis. This may help to explain the increased tryptophan levels measured in pumpkin hypocotyls after EOD-FR treatment [30].

Studies in *Arabidopsis* and other species have indicated that the polar auxin transport (PAT) system is essential for hypocotyl elongation in low R:FR environments [13]. The PAT system comprises a variety of auxin transporters, including both influx and efflux carriers [33]. These carriers have been shown to play an important role in the response to low R:FR and the induction of hypocotyl elongation. Takemura et al. (2016) found that PIN 4 was significantly upregulated by EOD-FR in Platycodon grandiflorum [34]. In the sav4 mutant, ABCB-mediated auxin efflux was blocked, and the response to low R:FR was significantly impaired [35]; likewise, hypocotyl elongation of ABCB19 deletion mutants was blocked under shade [36]. Moreover, a study on kidney bean (Phaseolus vulgaris) showed that the hypocotyl length of a PaLAX1 mutant was significantly shorter than that of the wild type [37]. This result showed that AUX-LIKE also plays an important role in the regulation of plant hypocotyl growth.

Using RNA-seq, we found that PIN 4, ABCB19, and several LAX genes were significantly upregulated after EOD-FR treatment. We also found that PIN-like 5 (PILS5) was downregulated 7.7-fold after EOD-FR. PILS5 localizes to the endoplasmic reticulum and participates in the dynamic balance of auxin in that organelle. Here, the expression of PILS5 was significantly downregulated after EOD-FR, suggesting a cumulative decrease in IAA in the ER, causing more IAA to flow into the nucleus and influence various biological processes [38].

The expression of other genes related to auxin transport was upregulated: a WALLS ARE THIN 1 (WAT1)-related gene [39] and two CBL-interacting serine/threonine protein kinase 6 (CIPK6)-related genes [40]. Based on previous studies, we speculate that changes in the expression of these genes enhanced transport of auxin to the hypocotyl, helping to explain the increased IAA content of this organ.

Studies have also shown that auxin homeostasis plays an important role in the regulation of hypocotyl IAA content [41]. GH3 and ILR1 influence auxin homeostasis in plants; for example, GH3.6 has been shown to regulate hypocotyl elongation in *Arabidopsis*, and hypocotyl length is shorter in its over-expression mutant [42]. ILR1 contributes to the hydrolysis of many auxin conjugates [43], and the *Arabidopsis* ilr1 mutant showed lower

IAA levels and shorter hypocotyls than the wild type [44]. Our RNA-seq data showed that the expression of GH3.6 decreased and that of ILR1 increased in pumpkin after EOD-FR treatment. These changes would be expected to increase IAA levels in the hypocotyl, in turn promoting its elongation.

Me-IAA was also detected in pumpkin in our study. Me-IAA is the methyl ester form of IAA [45] and participates in the homeostatic regulation of IAA in plants; its levels increased in pumpkin hypocotyls after EOD-FR treatment. Me-IAA is thought to be inactive in pumpkin seedlings [46], but it can recover its biological activity through conversion back to IAA, thereby increasing the level of IAA in pumpkin hypocotyls [45,46].

5. Conclusions

Our results suggest that auxin plays an essential role in EOD-FR-mediated hypocotyl elongation in pumpkin. In the presence of EOD-FR, there were changes in the expression of genes related to auxin synthesis, transport, and homeostasis, and these led to increased IAA content in pumpkin hypocotyls, promoted the expansion of hypocotyl cells, and ultimately caused significant hypocotyl elongation.

Supplementary Materials: The following are available online at https://www.mdpi.com/article/10.3390/agronomy11050853/s1. Figure S1: IAA and Me-IAA Linear equation and correlation coefficient of standard curve. Figure S2: Me-IAA levels in different treatments. Error bars represent $\pm$ SD. Different letters denote significant differences ($p < 0.05$). Figure S3: PCA analysis of metabolites identified in positive ion mode. Figure S3A: PCA score plots were derived from the relative contents of all metabolites detected by LC−MS/MS with six replicates per treatment. Figure S3B: PCA analysis of metabolites identified in negative ion mode. Figure S4A: Heatmap of all DEGs in CK vs. T pumpkin hypocotyls. Figure S5: Volcano plots of DEGs in pumpkin hypocotyls. Figure S6: GO enrichment scatter plot of DEGs in hypocotyls. Figure S7: KEGG enrichment scatter plot of DEGs in hypocotyls. Figure S8: Comparison of the log2(fold change) values of six EOD-FR-related DEGs measured by RNA-Seq and qRT–PCR. Figure S9: Correlations between qRT–PCR and RNA-seq data for the six DEGs. Each point represents a gene expression fold-change value in pumpkin hypocotyls. Table S1: Primer sequences used in qRT–PCR. Table S2: List of key metabolites associated with EOD-FR treatment. Table S3: RNA-seq statistics and quality control. Table S4: List of DEGs between control and EOD-FR-treated hypocotyls. Table S5: List of significantly enriched GO terms in DEGs between control and EOD-FR-treated hypocotyls. Table S6: List of significantly enriched KEGG pathways of DEGs between control and EOD-FR-treated hypocotyls.

Author Contributions: Q.L. (Qi Liu) and H.Z. performed the experiments; Z.Y. and Y.W. participated in experimental design and coordination; Y.M., Q.L. (Qi Li) and H.Y. collected the samples; Q.L. (Qi Liu), Z.Y., Y.B. and Y.W. drafted the manuscript; J.M., X.X., Q.L. (Qi Li) and Y.W. proofread and finalized the manuscript. All authors have read and agreed to the published version of the manuscript.

Institutional Review Board Statement: Not applicable.

Informed Consent Statement: Informed consent was obtained from all subjects involved in the study.

Conflicts of Interest: The authors declare no conflict of interest.

References

1. Chia, P.-L.; Kubota, C. End-of-day Far-red Light Quality and Dose Requirements for Tomato Rootstock Hypocotyl Elongation. *Hortscience* **2010**, *45*, 1501–1506. [CrossRef]
2. Bantis, F.; Smirnakou, S.; Ouzounis, T.; Koukounaras, A.; Ntagkas, N.; Radoglou, K. Current status and recent achievements in the field of horticulture with the use of light-emitting diodes (LEDs). *Sci. Hortic.* **2018**, *235*, 437–451. [CrossRef]
3. Bognar, L.K.; Hall, A.; Adam, E.; Thain, S.C.; Nagy, F.; Millar, A.J. The circadian clock controls the expression pattern of the circadian input photoreceptor, phytochrome B. *Proc. Natl. Acad. Sci. USA* **1999**, *96*, 14652–14657. [CrossRef] [PubMed]
4. Franklin, K.A. Shade avoidance. *New Phytol.* **2008**, *179*, 930–944. [CrossRef]

5. Mizuno, T.; Oka, H.; Yoshimura, F.; Ishida, K.; Yamashino, T. Insight into the mechanism of end-of-day far-red light (EODFR)-induced shade avoidance responses in Arabidopsis thaliana. *Biosci. Biotechnol. Biochem.* **2015**, *79*, 1987–1994. [CrossRef]

6. Yang, Z.-C.; Kubota, C.; Chia, P.-L.; Kacira, M. Effect of end-of-day far-red light from a movable LED fixture on squash rootstock hypocotyl elongation. *Sci. Hortic.* **2012**, *136*, 81–86. [CrossRef]

7. Xiong, J.Q.; Patil, G.G.; Moe, R. Effect of DIF and end-of-day light quality on stem elongation in Cucumis sativus. *Sci. Hortic.* **2002**, *94*, 219–229. [CrossRef]

8. Kalaitzoglou, P.; van Ieperen, W.; Harbinson, J.; van der Meer, M.; Martinakos, S.; Weerheim, K.; Nicole, C.C.S.; Marcelis, L.F.M. Effects of Continuous or End-of-Day Far-Red Light on Tomato Plant Growth, Morphology, Light Absorption, and Fruit Production. *Front. Plant. Sci.* **2019**, *10*, 322. [CrossRef]

9. Graham, H.A.H.; Decoteau, D.R. Young watermelon plant growth responses to end-of-day red and far-red light are affected by direction of exposure and plant part exposed. *Sci. Hortic.* **1997**, *69*, 41–49. [CrossRef]

10. Louws, F.J.; Rivard, C.L.; Kubota, C. Grafting fruiting vegetables to manage soilborne pathogens, foliar pathogens, arthropods and weeds. *Sci. Hortic.* **2010**, *127*, 127–146. [CrossRef]

11. Karaagac, O.; Balkaya, A. Interspecific hybridization and hybrid seed yield of winter squash (Cucurbita maxima Duch.) and pumpkin (Cucurbita moschata Duch.) lines for rootstock breeding. *Sci. Hortic.* **2013**, *149*, 9–12. [CrossRef]

12. Tao, Y.; Ferrer, J.-L.; Ljung, K.; Pojer, F.; Hong, F.; Long, J.A.; Li, L.; Moreno, J.E.; Bowman, M.E.; Ivans, L.J.; et al. Rapid synthesis of auxin via a new tryptophan-dependent pathway is required for shade avoidance in plants. *Cell* **2008**, *133*, 164–176. [CrossRef]

13. Keuskamp, D.H.; Pollmann, S.; Voesenek, L.A.C.J.; Peeters, A.J.M.; Pierik, R. Auxin transport through PIN-FORMED 3 (PIN3) controls shade avoidance and fitness during competition. *Proc. Natl. Acad. Sci. USA* **2010**, *107*, 22740–22744. [CrossRef] [PubMed]

14. Zhang, M.; Kong, X.; Xu, X.; Li, C.; Tian, H.; Ding, Z. Comparative Transcriptome Profiling of the Maize Primary, Crown and Seminal Root in Response to Salinity Stress. *PLoS ONE* **2015**, *10*, e0121222. [CrossRef] [PubMed]

15. Upadhyay, S.; Phukan, U.J.; Mishra, S.; Shukla, R.K. De novo leaf and root transcriptome analysis identified novel genes involved in Steroidal sapogenin biosynthesis in Asparagus racemosus. *BMC Genom.* **2014**, *15*, 1–13. [CrossRef]

16. Schwender, J.; Koenig, C.; Klapperstueck, M.; Heinzel, N.; Munz, E.; Hebbelmann, I.; Hay, J.O.; Denolf, P.; De Bodt, S.; Redestig, H.; et al. Transcript abundance on its own cannot be used to infer fluxes in central metabolism. *Front. Plant. Sci.* **2014**, *5*, 668. [CrossRef] [PubMed]

17. Bino, R.J.; Hall, R.D.; Fiehn, O.; Kopka, J.; Saito, K.; Draper, J.; Nikolau, B.J.; Mendes, P.; Roessner-Tunali, U.; Beale, M.H.; et al. Potential of metabolomics as a functional genomics tool. *Trends Plant Sci.* **2004**, *9*, 418–425. [CrossRef]

18. Iino, M. Gravitropism and phototropism of maize coleoptiles—Evaluation of the cholodny-went theory through effects of auxin application and decapitation. *Plant Cell Physiol.* **1995**, *36*, 361–367. [CrossRef]

19. Du, F.; Ruan, G.; Liu, H. Analytical methods for tracing plant hormones. *Anal. Bioanal. Chem.* **2012**, *403*, 55–74. [CrossRef]

20. Trapnell, C.; Williams, B.A.; Pertea, G.; Mortazavi, A.; Kwan, G.; van Baren, M.J.; Salzberg, S.L.; Wold, B.J.; Pachter, L. Transcript assembly and quantification by RNA-Seq reveals unannotated transcripts and isoform switching during cell differentiation. *Nat. Biotechnol.* **2010**, *28*, 511–515. [CrossRef]

21. Schmittgen, T.D.; Livak, K.J. Analyzing real-time PCR data by the comparative C-T method. *Nat. Protoc.* **2008**, *3*, 1101–1108. [CrossRef]

22. Jing, W.; Zhang, S.; Fan, Y.; Deng, Y.; Wang, C.; Lu, J.; Sun, X.; Ma, N.; Shahid, M.O.; Li, Y.; et al. Molecular Evidences for the Interactions of Auxin, Gibberellin, and Cytokinin in Bent Peduncle Phenomenon in Rose (Rosa sp.). *Int. J. Mol. Sci.* **2020**, *21*, 1360. [CrossRef]

23. Marklova, E. Where does indolylacrylic acid come from? *Amino Acids* **1999**, *17*, 401–413. [CrossRef]

24. Won, C.; Shen, X.; Mashiguchi, K.; Zheng, Z.; Dai, X.; Cheng, Y.; Kasahara, H.; Kamiya, Y.; Chory, J.; Zhao, Y. Conversion of tryptophan to indole-3-acetic acid by Tryptophan Aminotransferases of Arabidopsis and YUCCAS in Arabidopsis. *Proc. Natl. Acad. Sci. USA* **2011**, *108*, 18518–18523. [CrossRef] [PubMed]

25. Yamamoto, Y.; Kamiya, N.; Morinaka, Y.; Matsuoka, M.; Sazuka, T. Auxin biosynthesis by the YUCCA genes in rice. *Plant Physiol.* **2007**, *143*, 1362–1371. [CrossRef]

26. Stepanova, A.N.; Robertson-Hoyt, J.; Yun, J.; Benavente, L.M.; Xie, D.-Y.; Dolezal, K.; Schlereth, A.; Juergens, G.; Alonso, J.M. TAA1-mediated auxin biosynthesis is essential for hormone crosstalk and plant development. *Cell* **2008**, *133*, 177–191. [CrossRef] [PubMed]

27. Muller-Moule, P.; Nozue, K.; Pytlak, M.L.; Palmer, C.M.; Covington, M.F.; Wallace, A.D.; Harmer, S.L.; Maloof, J.N. YUCCA auxin biosynthetic genes are required for Arabidopsis shade avoidance. *PeerJ* **2016**, *4*, e2574. [CrossRef]

28. Peng, M.; Li, Z.; Zhou, N.; Ma, M.; Jiang, Y.; Dong, A.; Shen, W.-H.; Li, L. Linking Phytochrome-Interacting factor to Histone Modification in Plant Shade Avoidance. *Plant Physiol.* **2018**, *176*, 1341–1351. [CrossRef] [PubMed]

29. Casanova-Saez, R.; Voss, U. Auxin Metabolism Controls Developmental Decisions in Land Plants. *Trends Plant. Sci.* **2019**, *24*, 741–754. [CrossRef]

30. Maeda, H.; Dudareva, N. The Shikimate Pathway and Aromatic Amino Acid Biosynthesis in Plants. *Annu. Rev. Plant Biol.* **2012**, *63*, 73–105. [CrossRef] [PubMed]

31. Matsuda, F.; Yamada, T.; Miyazawa, H.; Miyagawa, H.; Wakasa, K. Characterization of tryptophan-overproducing potato transgenic for a mutant rice anthranilate synthase alpha-subunit gene (OASA1D). *Planta* **2005**, *222*, 535–545. [CrossRef]

32. Morino, K.; Matsuda, F.; Miyazawa, H.; Sukegawa, A.; Miyagawa, H.; Wakasa, K. Metabolic profiling of tryptophan-overproducing rice calli that express a feedback-insensitive alpha subunit of anthranilate synthase. *Plant Cell Physiol.* **2005**, *46*, 514–521. [CrossRef]

33. Grones, P.; Friml, J. Auxin transporters and binding proteins at a glance. *J. Cell Sci.* **2015**, *128*, 1–7. [CrossRef] [PubMed]

34. Takemura, Y.; Kuroki, K.; Katou, M.; Kishimoto, M.; Tsuji, W.; Nishihara, E.; Tamura, F. Gene expression changes triggered by end-of-day far-red light treatment on early developmental stages of Eustoma grandiflorum (Raf.) Shinn. *Sci. Rep.* **2015**, *5*, 1–11. [CrossRef] [PubMed]

35. Ge, Y.; Yan, F.; Zourelidou, M.; Wang, M.; Ljung, K.; Fastner, A.; Hammes, U.Z.; Di Donato, M.; Geisler, M.; Schwechheimer, C.; et al. Shade Avoidance 4 Is Required for Proper Auxin Distribution in the Hypocotyl. *Plant Physiol.* **2017**, *173*, 788–800. [CrossRef] [PubMed]

36. Wu, G.; Carville, J.S.; Spalding, E.P. ABCB19-mediated polar auxin transport modulates Arabidopsis hypocotyl elongation and the endoreplication variant of the cell cycle. *Plant J.* **2016**, *85*, 209–218. [CrossRef] [PubMed]

37. Hoyerova, K.; Perry, L.; Hand, P.; Lankova, M.; Kocabek, T.; May, S.; Kottova, J.; Paces, J.; Napier, R.; Zazimalova, E. Functional characterization of PaLAX1, a putative auxin permease, in heterologous plant systems. *Plant Physiol.* **2008**, *146*, 1128–1141. [CrossRef]

38. Titapiwatanakun, B.; Blakeslee, J.J.; Bandyopadhyay, A.; Yang, H.; Mravec, J.; Sauer, M.; Cheng, Y.; Adamec, J.; Nagashima, A.; Geisler, M.; et al. ABCB19/PGP19 stabilises PIN1 in membrane microdomains in Arabidopsis. *Plant J.* **2009**, *57*, 27–44. [CrossRef] [PubMed]

39. Ranocha, P.; Dima, O.; Nagy, R.; Felten, J.; Corratge-Faillie, C.; Novak, O.; Morreel, K.; Lacombe, B.; Martinez, Y.; Pfrunder, S.; et al. Arabidopsis WAT1 is a vacuolar auxin transport facilitator required for auxin homoeostasis. *Nat. Commun.* **2013**, *4*, 1–9. [CrossRef]

40. Tripathi, V.; Parasuraman, B.; Laxmi, A.; Chattopadhyay, D. CIPK6, a CBL-interacting protein kinase is required for development and salt tolerance in plants. *Plant J.* **2009**, *58*, 778–790. [CrossRef]

41. Ljung, K. Auxin metabolism and homeostasis during plant development. *Development* **2013**, *140*, 943–950. [CrossRef] [PubMed]

42. Takase, T.; Nakazawa, M.; Ishikawa, A.; Kawashima, M.; Ichikawa, T.; Takahashi, N.; Shimada, H.; Manabe, K.; Matsui, M. ydk1-D, an auxin-responsive GH3 mutant that is involved in hypocotyl and root elongation. *Plant J.* **2004**, *37*, 471–483. [CrossRef] [PubMed]

43. Bartel, B.; Fink, G.R. ILR1, an amidohydrolase that releases active indole-3-acetic-acid from conjugates. *Science* **1995**, *268*, 1745–1748. [CrossRef] [PubMed]

44. Rampey, R.A.; LeClere, S.; Kowalczyk, M.; Ljung, K.; Sandberg, G.; Bartel, B. A family of auxin-conjugate hydrolases that contributes to free indole-3-acetic acid levels during Arabidopsis germination. *Plant Physiol.* **2004**, *135*, 978–988. [CrossRef] [PubMed]

45. Jiang, Z.; Liu, D.; Wang, T.; Liang, X.; Cui, Y.; Liu, Z.; Li, W. Concentration difference of auxin involved in stem development in soybean. *J. Integr. Agric.* **2020**, *19*, 953–964. [CrossRef]

46. Li, J.; Li, C.; Smith, S.M.; Li, J.; Li, C.; Smith, S.M. *Hormone Metabolism and Signaling in Plants*; Academic Press: Cambridge, MA, USA, 2017.